Waveform inversion for S-wave structure in the lowermost mantle beneath the Arctic: Implications for mineralogy and chemical composition

Kenji Kawai,[1,2] Robert J. Geller,[3] and Nobuaki Fuji[3,4]

Received 19 April 2010; revised 12 June 2010; accepted 17 June 2010; published 17 August 2010.

[1] We perform waveform inversion for the radial profile of shear wave velocity in the lowermost mantle beneath the Arctic. We use waveforms from the CANOE (CAnadian NOrthwest Experiment) array, which greatly enhances the resolution in the lowermost mantle as compared to earlier studies. We find a velocity increase at depths from 2500 to 2700 km and a velocity decrease at depths from 2700 km to the core-mantle boundary (CMB). We interpret the velocity increase as associated with the phase transition from perovskite (pv) to post-perovskite (ppv), and the velocity decrease as due to a temperature increase in the thermal boundary layer. The shear wave velocity immediately above the core-mantle boundary (CMB) is 7.11 km/s, while that beneath Central America is 7.25 km/s. This suggests that the proportion of impurities in Mg-pv or Mg-ppv beneath the Arctic is 6 mol% larger than that beneath Central America.
Citation: Kawai, K., R. J. Geller, and N. Fuji (2010), Waveform inversion for S-wave structure in the lowermost mantle beneath the Arctic: Implications for mineralogy and chemical composition, *Geophys. Res. Lett.*, *37*, L16301, doi:10.1029/2010GL043654.

1. Introduction

[2] As the seismic structure within the D″ region cannot be resolved by travel-time tomography, it is important to investigate the structure of the lowermost mantle in detail using waveform inversion. We have developed methods to invert seismic waveforms for localized seismic structure and applied these methods to infer the shear wave velocity within D″. We have studied regions with both high [*Kawai et al.*, 2007a, 2007b, 2009] and low [*Konishi et al.*, 2009; *Kawai and Geller*, 2010] average velocity. The former studies found that high velocities are concentrated in the upper half of the D″ region and that there is a steep negative velocity gradient in the lower half of D″. On the other hand, the latter studies found an "S-shaped" velocity profile, which has a low S-velocity zone in the depth range from 2550 to 2750 km. Both structures can be explained by simple thermal effects for a temperature at the CMB of 3800 K [*Kawai and Tsuchiya*, 2009]. In this study we determine the shear wave velocity structure in the lowermost mantle beneath the Arctic, and compare it to the shear wave velocity immediately above the CMB beneath Central Asia, Central America, and the Pacific to estimate the respective proportion of impurities in Mg-pv (perovskite) or Mg-ppv (post-perovskite).

2. Analysis

[3] The regions beneath which the structure of D″ can be studied in detail are limited due to the source and receiver geometry. *Kawai et al.* [2007b] studied the shear velocity structure beneath the Arctic using Sd waveforms for many stations for seven events as well as a small number of S waveforms. They showed that while long-period Sd data could constrain the average structure in D″ and suggest the existence of two-layered structure, waveforms from stations at epicentral distances $70° < \Delta < 90°$ are required to quantitatively constrain the fine structure within D″.

[4] A temporary seismic array, CANOE (CAnadian NOrthwest Experiment), was deployed in northwest Canada for two and a half years from 2003 to 2005. The CANOE array provides waveform data at epicentral distances around 80° from intermediate-depth events beneath the Hindu-Kush region. In this study we invert for the fine structure of the lowermost mantle beneath the Arctic using S-wave waveforms, including recordings from the CANOE array. Although CANOE data for Hindu-Kush events have a low S/N ratio, waveform inversion can treat such noisy data.

2.1. Waveform Data

[5] We use the transverse components of broadband waveform data (obtained by rotating the N-S and E-W components) for 7 events from the IRIS and CNSN data centers (Table 1 and Figure 1a). Stations in North America including the CANOE array were chosen (Figure 1b). The CANOE stations recorded waveforms for 3 of the 7 events (shown in Table 1). We deconvolve the instrument response and apply a bandpass filter to the data and construct data sets for the period range 8–200 s. We then select records which include data for S, ScS and the other phases which arrive between them at epicentral distances $\Delta < 100°$. We compute the ratio of the maximum amplitude of the data and the corresponding synthetic, and eliminate records for which the ratio is greater than 2 or less than 0.5. The dataset consists of 232 records that satisfy the above criteria; 213 records which did not satisfy the criteria were rejected. The data are velocity seismograms (with units of m/s after deconvolving the instrument response) with 1 Hz sampling. The reciprocal of the maximum amplitude of each record is used as the weighting factor in the inversion, so that all data have roughly the same importance.

[1]Department of Earth and Planetary Sciences, Tokyo Institute of Technology, Tokyo, Japan.
[2]Institut de Physique du Globe de Paris, Paris, France.
[3]Department of Earth and Planetary Science, Graduate School of Science, Tokyo University, Tokyo, Japan.
[4]Now at Laboratoire de Dynamique Terrestre et Planétaire, Observatoire Midi-Pyrénées, Université de Tolouse, Toulouse, France.

0094-8276/10/2010GL043654

Table 1. Earthquakes Used in This Study

Event	Date (Y/M/D)	Latitude	Longitude	Depth	M_w
1	2000/5/1	37.82°	72.43°	152.0	5.6
2	2001/2/25	36.41°	70.62°	193.4	6.1
3[a]	2004/4/5	36.52°	70.84°	183.5	6.5
4[a]	2004/8/10	36.52°	70.60°	205.7	6.0
5[a]	2005/7/23	36.40°	70.65°	212.9	5.5
6	2005/12/12	36.45°	71.06°	210.2	6.5
7	2007/4/3	36.57°	70.59°	221.4	6.2

[a]Event observed by the CANOE array.

[6] The source parameters (moment tensors and centroids) are fixed to the Global CMT solution. *Kawai et al.* [2007a] approximated the source time function as a δ-function at the centroid time for the period range 20–200 s. As this study, however, uses data for the period range 8–200 s, we use boxcar moment rate functions whose half-duration is obtained from the Global CMT solutions. We convolve the boxcar moment rate function with the synthetic seismograms and their partial derivatives in the frequency domain.

[7] Waveforms that sample the lowermost mantle pass through the crust, upper mantle, transition zone, and lower mantle, whose effects must be corrected for. We handle this by determining static corrections (time shifts) for the observed waveforms. As only three of the Hindu-Kush events were observed by CANOE stations, this study cannot use the methods of *Kawai and Geller* [2010], whereby the time shifts for events and stations are simultaneously inferred together with the parameters of the Earth model. Following *Fuji et al.* [2010], we make static corrections using the time shift that gives the best correlation coefficient between the synthetic and observed seismograms, using the arrivals of direct S waves as the reference.

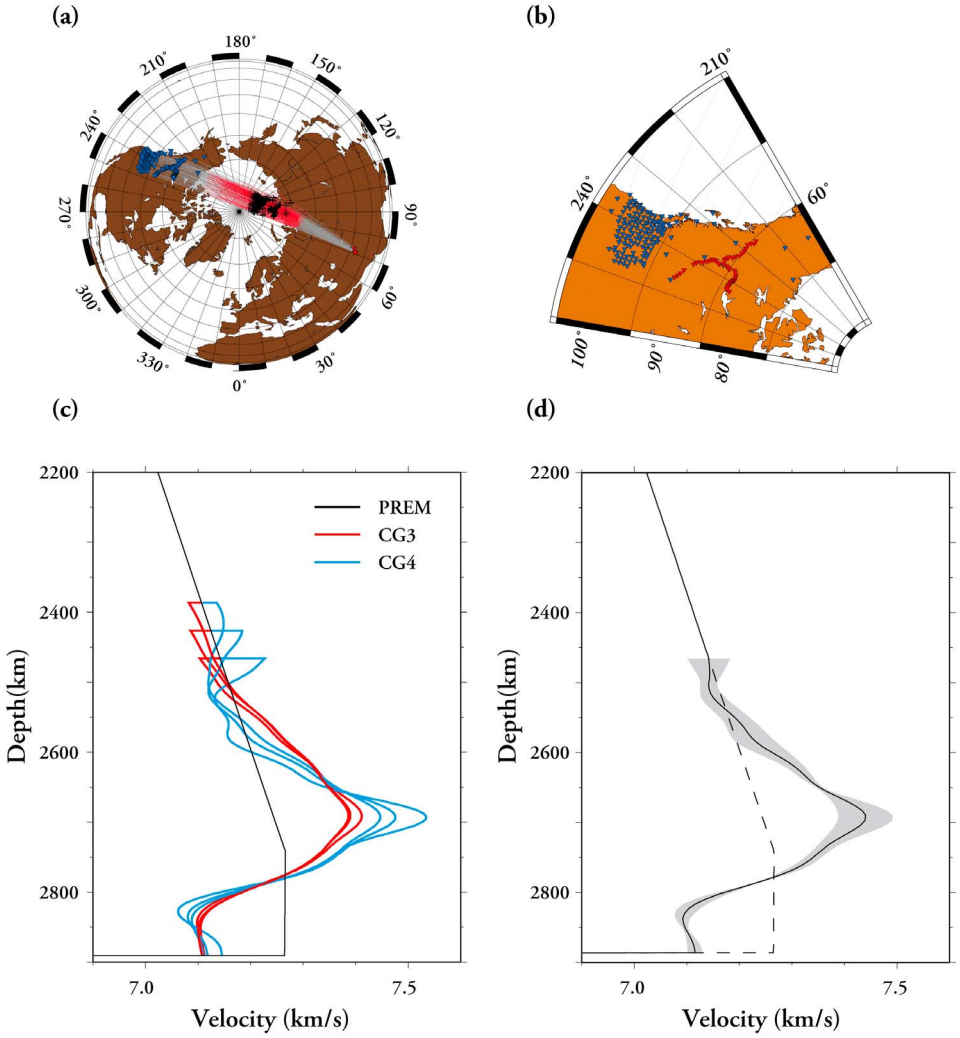

Figure 1. (a) Event-receiver geometry, with great circle ray paths. The ray-paths are shown to indicate the coverage, but note that we do not use ray-theoretical approximations. The portions of the great circles which sample D″ are shown in red. Blue reversed triangles and red stars show the sites of stations used in our study and earthquakes studied, respectively. (b) Detailed map of the stations used. CANOE stations are shown by red triangles and permanent stations by blue triangles. (c) The results of inversions for tie-in depths of 420, 460, and 500 km above the CMB for bases of the first 3 or 4 CG vectors, respectively. (d) Nominal error bars (one standard deviation) estimated by treating the six CG models in Figure 1c as independent.

Table 2. Variance and AIC for Each Model[a]

Model	Variance (%)	AIC
PREM	183.6	2857.8
PREM with time shift	127.1	2607.1
CG3 (460 km)	106.7	2465.0
CG4 (460 km)	106.1	2462.3
CG3 (480 km)	107.1	2467.6
CG4 (480 km)	106.3	2463.5
CG3 (500 km)	107.1	2468.3
CG4 (500 km)	106.4	2464.5

[a]The total number of data points is 16577.

2.2. Waveform Inversion

[8] For the details of our inversion methods see *Konishi et al.* [2009], *Kawai and Geller* [2010], *Fuji et al.* [2010], *Fuji* [2010], and the references cited therein. Our inversion is a linearized inversion, with the perturbation to the Earth model in the target zone and the time shifts (static corrections) as the variables. We determine the model parameters by minimizing AIC (Akaike's Information Criterion [*Akaike*, 1977]), which rewards variance reduction and penalizes increases in the complexity of the model. The initial model is anisotropic PREM [*Dziewonski and Anderson*, 1981]. The source parameters (moment tensors, centroids and half-durations) are fixed to the Global CMT solution. In this study, the S-wave velocities at points above the 'tie-in depth' are fixed to PREM, while those below the tie-in depth are the unknown parameters. We conduct inversions using the first n vectors of the conjugate gradient (CG) decomposition of the matrix of coefficients of the normal equations as the basis functions (see *Fuji* [2010] for details). We vary two parameters to examine the robustness of the inversion results (Figure 1c). First, we invert respectively for tie-in depths of 420, 460, and 500 km above the CMB. Second, we invert for models using the first 3 and 4 vectors of the CG decomposition as the basis; these models are labeled CG3 and CG4, respectively.

[9] Table 2 shows the variance (computed using the Born approximation) for the various inversions. Defining the variance of the data to be 100%, the variance of the residuals (data − PREM synthetics) is 183.6%. A further variance reduction (to 127.1%) is achieved by making the time shift corrections. The variance values for the six models obtained by the CG inversions are in the range from 106.1% to 107.1%. Since the velocities at points above the tie-in depth are fixed to the initial model (PREM), the residual error is, at least in part, due to the differences between the real Earth and the Earth model (including Q) outside the study region, and also to source effects. Table 2 also shows the values of AIC for each model. We assume that the effective number of independent data is 12.5% (1/8) of the above number of data points, 16577, because the data are sampled at 1 Hz but are low-passed filtered to exclude periods shorter than 8 s. The lower values of AIC in Table 2 for "PREM with time shift" (as compared to PREM), and for the six CG models (as compared to "PREM with time shift") show the formal statistical significance of the respective models.

[10] We briefly discuss the magnitude of the variance values shown in Table 2. In the case of, for example, a parametric fitting of some curve (e.g., a straight line) to observed data, a variance of over 100% might appear unacceptably large. But in this case the variance values in Table 2 are for the fit of broadband synthetics to observed waveforms. Furthermore, there is a total of 16,577 data points in the various time series, and only three or four free parameters (the coefficients of the CG basis vectors in the perturbation to the starting model), so (as is confirmed by AIC) the variance reduction for the CG models is statistically significant, notwithstanding the fact that the final variance is on the order of 100%.

[11] Figure 1c shows that all six of the CG models have basically the same general depth-dependence. There is a velocity increase in the depth range 2500–2700 km and a relative velocity decrease in the depth range from 2700 km to the CMB. The general pattern of the increase and decrease is compatible with our previous results [*Kawai et al.*, 2007b] for D″ beneath the Arctic. As all six models produce roughly the same variance reduction, the differences between these models can be regarded as giving a rough indication of the uncertainty of the inversion results (Figure 1d). The shaded zone is one nominal standard deviation, taking the six models as independent data. (As is well known, the actual error may well be greater than the nominal error estimates.) The velocity increase and decrease are considerably in excess of the nominal error estimates. *Fuji* [2010] conducted a detailed analysis of waveform inversion for the upper mantle and mantle transition structure near Japan, and demonstrated that despite the large variance for each individual record a reliable and consistent model was obtained. This conclusion applies to waveform inversion in general.

[12] We prepared "quality control (QC) stacks," shown in Figure 2, for each of the seven events analyzed by this study. QC stacks are not intended for use in obtaining the Earth model, but rather as an ancillary check to confirm that the inversion result is reasonable. The stacks are made by aligning and summing the records (after static corrections), using the PREM arrival time and normalizing the maximum amplitude of each of the observed records to one. Because a non-causal filter is used, there are signals before time $t = 0$. The synthetics (computed for model CG4, with a tie-in depth of 500 km) are processed using the same weighting factors as the corresponding observed records.

[13] The QC stacks in Figure 2 show that the synthetics for the final model are, overall, a clear improvement over the initial model, thereby confirming that the inversion has reached a reasonable result. The stacked data show ringing (presumably due to secondary scattering due to heterogeneity throughout the Earth) that is not present in the synthetics for either PREM or our final model. Also, there are in some cases significant amplitude differences, presumably due to both anelastic attenuation and focusing/defocusing effects. Figure 2 shows the ability of waveform inversion to obtain robust Earth models from data which are too noisy to permit analysis by trial and error forward modeling. To study the uncertainty of our models and the resolving power of our inversions, and to present further visual examples of observed and synthetic seismograms, additional material is presented in the auxiliary material.[1]

3. Discussion

[14] The average composition in the mantle is thought to contain impurities such as aluminum and iron [*Ringwood*,

[1]Auxiliary materials are available in the HTML. doi:10.1029/2010GL043654.

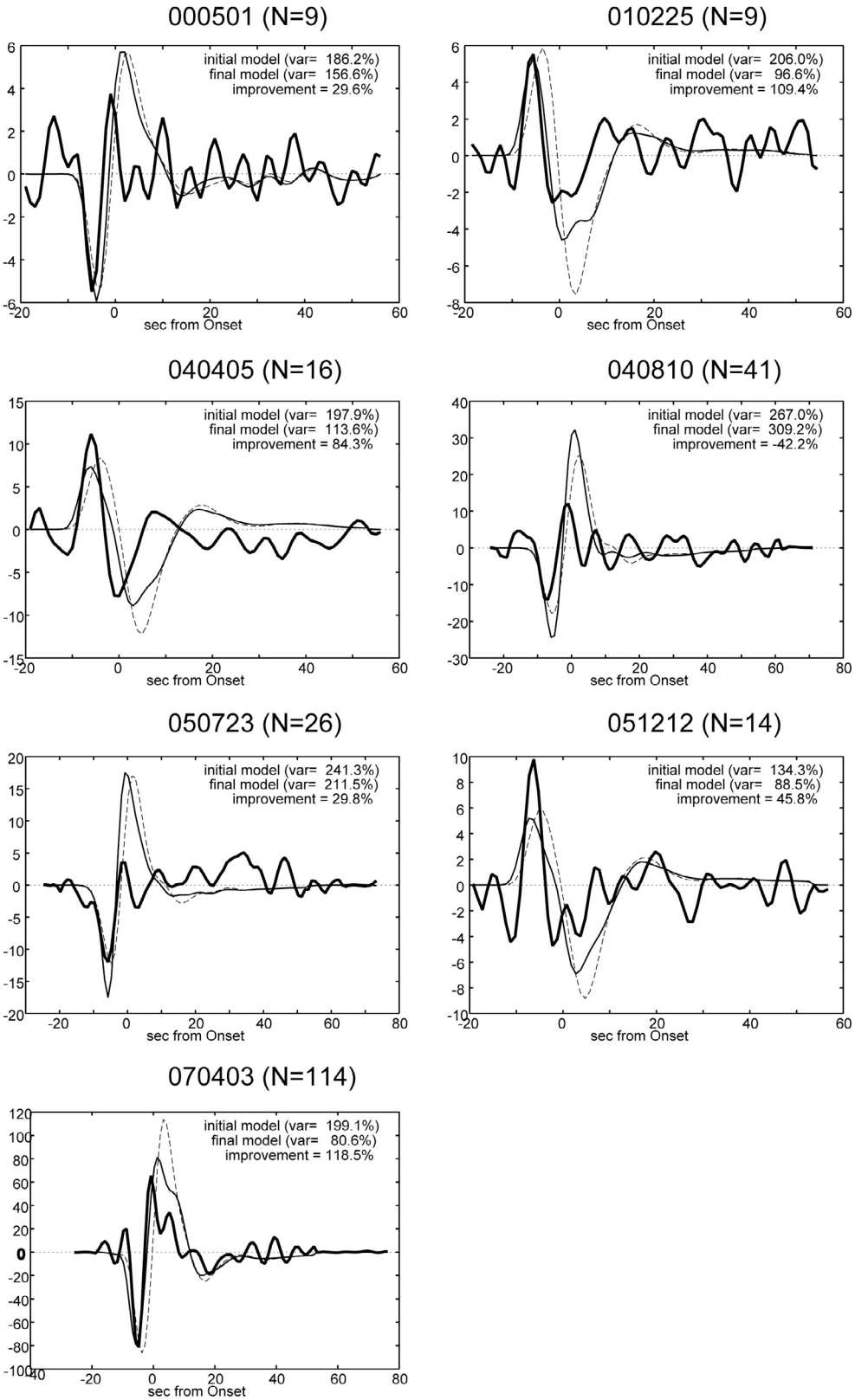

Figure 2. Quality control (QC) stacks for each of the seven events, which were computed as follows. First, all of the observed waveforms for each event which met the selection criteria were time shifted using PREM, after making the same static corrections as in the inversion. These waveforms were then filtered in the passband 8 s to 200 s using a four-pole non-causal bandpass filter. The maximum amplitude of each observed record was normalized to one, and the waveforms were then stacked (thick curves). The synthetics for the initial model (PREM, dotted curves) and final model (model CG4, for a tie-in depth of 500 km) (thin solid curves) were stacked using the same weighting factors as for the corresponding observed record.

1962]. Arguments from mineral physics show that impurities in Mg-pv decrease the shear wave velocity [*Tsuchiya and Tsuchiya*, 2006]. For example, a 1 mol% increase in the amount of both aluminum and iron causes a 0.303% velocity decrease in Mg-pv or a 0.367% velocity decrease in Mg-ppv. In this study we estimated the shear wave velocity as about 7.11 km/s immediately above the CMB. As the temperature at the CMB is isothermal, the shear wave velocity at the CMB would be equal everywhere if the mineralogical phase and chemical composition is identical [*Kawai and Tsuchiya*, 2009]. Since seismic velocity can be directly inferred by waveform inversion, we can use the inferred velocity immediately above the CMB to distinguish the effects of temperature from those of chemical composition.

[15] Our previous study of D″ beneath Central America [*Kawai et al.*, 2007a] found an S-wave velocity of about 7.25 km/s immediately above the CMB, which is about 0.14 km/s faster than the velocity obtained in this study. This difference can be interpreted as due to the amount of impurities in Mg-ppv beneath the Arctic being 6 mol% larger than that beneath Central America, on the assumption that the ratio of aluminum and iron is constant in Mg-ppv. As PREM can be approximated as pyrolitic composition with 7 mol% impurities [*McDonough and Sun*, 1995], we therefore estimate the amount of impurities in Mg-ppv beneath the Arctic to be 13 mol%. *Konishi et al.* [2009] found a shear velocity of 7.18 km/s immediately above the CMB in the western Pacific, which can be interpreted as suggesting that the amount of impurities in Mg-ppv is 3 mol% larger there than that beneath Central America. *Kawai et al.* [2009] found a shear velocity of 7.22 km/s at the CMB beneath Central Asia, suggesting that the amount of impurities in Mg-ppv is 1 mol% larger there than beneath central America.

[16] Impurities in D″ would cause a two-phase coexistence region for the pv to ppv phase transition. The existence of a two-phase coexistence region has been studied experimentally, for example, in the majorite-perovskite system [*Irifune et al.*, 1996; *Hirose et al.*, 1999] and the pv-ppv system [*Tateno et al.*, 2007; *Ohta et al.*, 2008]. In multi-component systems in natural compositions such as pyrolite and MORB (mid-ocean ridge basalt) the width of the two-phase coexistence region due to complexities of mineralogy at mantle pressures [*Hirose et al.*, 1999; *Ohta et al.*, 2008] is narrower than that in the $MgSiO_3$-Al_2O_3 and the $MgSiO_3$-$FeSiO_3$ systems [*Ohtani and Sakai*, 2008]. Recent studies on mineral physics show that the width of the two-phase coexistence region is as narrow in the $MgSiO_3$-Al_2O_3 system [*Tsuchiya and Tsuchiya*, 2008] as seismically detectable discontinuities.

[17] The model obtained in this study shows a velocity increase in the depth range from 2500 to 2700 km. This velocity increase is consistent with the experimental result that the post-perovskite phase transition in pyrolitic mantle occurs between 116 and 122 GPa, corresponding to the depth range from 2550 to 2640 km [*Ohta et al.*, 2008]. While the experiments predict a width of about 90 km, our model shows a width of about 200 km. A resolution test (Figure S2 of the auxiliary material) suggests that a step function discontinuity would result in an apparent transition depth of 100 km in the seismic velocity models inferred by our methods for the period band used in this study. The 200 km transition in Figure 1c is thus consistent with a transition over a 100 km depth range, but this is not conclusive. However, when taken together with the extremely low (7.11 km/s) S-velocity just above the CMB, our data are consistent with the presence of significant impurities in D″ beneath the Arctic. Taking into account the resolution of our dataset shown in Figure S2, we cannot exclude the possibility of a higher temperature in the depth range from 100 km above the CMB to the CMB produced by a hypothetical blanketing effect.

[18] As shown in Figure 1d, the nominal error of the shear velocity immediately above the CMB obtained by this study is about ±0.02 km/s. If we assume the uncertainty of the velocities immediately above the CMB obtained by the other studies cited above is of comparable order, the difference between the various regions is well in excess of the nominal uncertainty. Further quantification of the uncertainties of the inferred velocities is an important subject for future work. The velocity decrease in the depth range from 2700 km to the CMB can be interpreted as due to the temperature increase in the thermal boundary layer of mantle convection [*Kawai and Tsuchiya*, 2009], because if a reverse phase transition from ppv to pv occurs due to a temperature increase (a possibility suggested by *Hernlund et al.* [2005]), the shear velocity at the CMB would be even lower (well below 7.0 km/s).

[19] **Acknowledgments.** We thank Taku Tsuchiya, Shigehiko Tateno and John Hernlund for valuable discussions. We also thank Sean Ford for informing us of the availability of CANOE array. Data were obtained from IRIS and CNSN data servers. KK and NF are supported by JSPS Fellowships for Young Scientists. This research was supported by a grant from the JSPS (22540433).

References

Akaike, H. (1977), An extension of the method of maximum likelihood and the Stein's problem, *Ann. Inst. Stat. Math.*, *29*, 153–164.

Dziewonski, A. M., and D. L. Anderson (1981), Preliminary reference Earth model, *Phys. Earth Planet. Inter.*, *25*, 297–356.

Fuji, N. (2010), A methodology for inversion of seismic waveforms for elastic and anelastic structure and its preliminary application to the mantle transition zone beneath the northwestern Pacific, Ph.D. thesis, Univ. of Tokyo, Tokyo.

Fuji, N., K. Kawai, and R. J. Geller (2010), A methodology for inversion of broadband seismic waveforms for elastic and anelastic structure and its application to the mantle transition zone beneath the northwestern Pacific, *Phys. Earth Planet. Inter.*, *180*, 118–137.

Hernlund, J. W., C. Thomas, and P. J. Tackley (2005), A doubling of the post-perovskite phase boundary and structure of the Earth's lowermost mantle, *Nature*, *434*, 882–886.

Hirose, K., Y. Fei, Y. Ma, and H.-K. Mao (1999), The fate of subducted basaltic crust in the Earth's lower mantle, *Nature*, *397*, 53–56.

Irifune, T., T. Koizumi, and J. Ando (1996), An experimental study of the garnet-perovskite transformation in the system $MgSiO_3$-$Mg_3A_2Si_3O_{12}$, *Phys. Earth Planet. Inter.*, *96*, 147–157.

Kawai, K., and R. J. Geller (2010), Waveform inversion for localized seismic structure and an application to D″ structure beneath the Pacific, *J. Geophys. Res.*, *115*, B01305, doi:10.1029/2009JB006503.

Kawai, K., and T. Tsuchiya (2009), Temperature profile in the lowermost mantle from seismological and mineral physics joint modeling, *Proc. Natl. Acad. Sci. U. S. A.*, *106*, 22,119–22,123.

Kawai, K., N. Takeuchi, R. J. Geller, and N. Fuji (2007a), Possible evidence for a double crossing phase transition in D″ beneath Central America from inversion of seismic waveforms, *Geophys. Res. Lett.*, *34*, L09314, doi:10.1029/2007GL029642.

Kawai, K., R. J. Geller, and N. Fuji (2007b), D″ beneath the Arctic from inversion of shear waveforms, *Geophys. Res. Lett.*, *34*, L21305, doi:10.1029/2007GL031517.

Kawai, K., S. Sekine, N. Fuji, and R. J. Geller (2009), Waveform inversion for D″ structure beneath northern Asia using Hi-net tiltmeter data, *Geophys. Res. Lett.*, *36*, L20314, doi:10.1029/2009GL039651.

Konishi, K., K. Kawai, R. J. Geller, and N. Fuji (2009), MORB in the lowermost mantle beneath the western Pacific: Evidence from waveform inversion, *Earth Planet. Sci. Lett.*, *278*, 219–225.

McDonough, W. F., and S. Sun (1995), The composition of the Earth, *Chem. Geol.*, *120*, 223–253.

Ohta, K., K. Hirose, T. Lay, N. Sata, and Y. Ohishi (2008), Phase transitions in pyrolite and MORB at lowermost mantle conditions: Implications for a MORB-rich pile above the core-mantle boundary, *Earth Planet. Sci. Lett.*, *267*, 107–117.

Ohtani, E., and T. Sakai (2008), Recent advances in the study of mantle phase transitions, *Phys. Earth Planet. Inter.*, *170*, 240–247.

Ringwood, A. E. (1962), A model for the upper mantle, *J. Geophys. Res.*, *67*, 857–867.

Tateno, S., K. Hirose, N. Sata, and Y. Ohishi (2007), Solubility of FeO in $(Mg,Fe)SiO_3$ perovskite and post-perovskite phase transition, *Phys. Earth Planet. Inter.*, *160*, 319–325.

Tsuchiya, J., and T. Tsuchiya (2008), Postperovskite phase equilibria in the $MgSiO_3$-Al_2O_3 system, *Proc. Natl. Acad. Sci. U. S. A.*, *105*, 19,160–19,164.

Tsuchiya, T., and J. Tsuchiya (2006), Effect of impurity on the elasticity of perovskite and postperovskite: Velocity contrast across the postperovskite transition in $(Mg,Fe,Al)(Si,Al)O_3$, *Geophys. Res. Lett.*, *33*, L12S04, doi:10.1029/2006GL025706.

N. Fuji, Laboratoire de Dynamique Terrestre et Planétaire, Observatoire Midi-Pyrénées, Université de Tolouse, CNRS, F-31400 Toulouse CEDEX, France.

R. J. Geller, Department of Earth and Planetary Science, Graduate School of Science, Tokyo University, Hongo 7-3-1, Bunkyo, Tokyo 113-0033, Japan.

K. Kawai, Department of Earth and Planetary Sciences, Tokyo Institute of Technology, Ookayama 2-12-1, Meguro, Tokyo 152-8551, Japan. (kenji@geo.titech.ac.jp)